Aging of basalt volcanic systems and decreasing CO_2 consumption by weathering

Janine Börker[1], Jens Hartmann[1], Gibran Romero-Mujalli[1], Gaojun Li[2]

[1]Institute for Geology, CEN (Center for Earth System Research and Sustainability), Universität Hamburg, Bundesstraße 55, 20146 Hamburg, Germany. E-Mail: janine.boerker@uni-hamburg.de; geo@hattes.de

[2]MOE Key Laboratory of Surficial Geochemistry, Department of Earth Sciences, Nanjing University, 163 Xianlindadao, Nanjing 210023, China

Abstract

Basalt weathering is one of many relevant processes balancing the global carbon cycle via land-ocean alkalinity fluxes. The CO_2 consumption by weathering can be calculated using alkalinity and is often scaled with runoff and/or temperature. Here it is tested if the surface age distribution of a volcanic system derived by geological maps is a useful proxy for changes in alkalinity production with time.

A linear relationship between temperature normalized alkalinity fluxes and the Holocene area fraction of a volcanic field was identified, using information from 33 basalt volcanic fields, with an $r^2=0.93$. This relationship is interpreted as an aging function and suggests that fluxes from Holocene areas are ~10 times higher than those from old inactive volcanic fields. However, the cause for the decrease with time is probably a combination of effects, including a decrease in alkalinity production from material in the shallow critical zone as well as a decline in hydrothermal activity and magmatic CO_2 contribution. The addition of fresh reactive material on top of the critical zone has an effect in young active volcanic settings which should be accounted for, too.

A comparison with global models suggests that global alkalinity fluxes considering Holocene basalt areas are ~60% higher than the average from these models imply. The contribution of Holocene areas to the global basalt alkalinity fluxes is today however only ~5%, because identified, mapped Holocene basalt areas cover only ~1% of the existing basalt areas. The large trap basalt proportion on the global basalt areas today reduces the relevance of the aging effect. However, the aging effect might be a relevant process during periods of globally, intensive volcanic activity, which remains to be tested.

1. Introduction

Basalt areas, despite their limited areal coverage, contribute significantly to CO_2 sequestration by silicate rock weathering (Gaillardet et al., 1999; Dessert et al., 2003; Hartmann et al., 2009). The sensitivity of basalt weathering to climate change (Dessert et al., 2001; Dessert et al., 2003; Coogan and Dosso, 2015; Li et al., 2016) supports a negative weathering feedback in the carbon cycle that

34 maintains the habitability of the Earth's surface over geological time scales (Walker et al., 1981;
35 Berner et al., 1983; Li and Elderfield, 2013). Changes in volcanic weathering fluxes due to
36 emplacement of large volcanic provinces or shifts in the geographic distribution of volcanic fields
37 associated with continental drift may have contributed to climate change in the past (Goddéris et
38 al., 2003; Schaller et al., 2012; Kent and Muttoni, 2013).

39 The role of basalt weathering in the carbon cycle and its feedback strength in the climate system
40 depends, besides the release of geogenic nutrients, on the amount of associated CO_2 consumption
41 and related alkalinity fluxes. The factors that module these fluxes are a subject to uncertainty.
42 Previous studies suggest that basalt weathering contributes 25–35% to the global silicate CO_2
43 consumption by weathering (Gaillardet et al., 1999; Dessert et al., 2003; Hartmann et al., 2009).
44 However, their estimations do not consider the potential aging of a weathering system (e.g., Taylor
45 and Blum, 1995). Young volcanic areas can show much higher weathering rates compared to older
46 ones, as was shown for the Lesser Antilles, where a rapid decay of weathering rates within the first
47 0.5 Ma was observed (Rad et al., 2013). Such an aging effect of volcanic areas is difficult to
48 parameterize for global basalt weathering fluxes, due to a lack of global compilations.

49 A practical approach to resolve this issue is to distinguish older and inactive volcanic fields (IVF)
50 and active volcanic fields (AVF) (Li et al., 2016) and compare weathering fluxes with factors
51 driving the weathering process, like land surface temperature or hydrological parameters. By
52 compiling data from 37 basaltic fields globally, Li et al. (2016) showed that spatially explicit
53 alkalinity fluxes (or CO_2 consumption rates) associated with basalt weathering correlate strongly
54 with land surface temperature for IVFs, but not for AVFs. They suggested that previously observed
55 correlations between weathering rates and runoff in global datasets originates partly from the
56 coincidence of high weathering rates and high runoff of AVFs rather than a direct primary runoff
57 control on the weathering rate. Many studied AVFs are located near the oceans and have an
58 elevated topography, a combination, which can cause elevated runoff due to an orographic effect
59 (Gaillardet et al., 2011). However, the effect of aging on weathering rates from a volcanic system
60 discussed here has not been evaluated.

61 The age distribution of the surface area of a whole volcanic system might be used as a first order
62 proxy to study the variability of weathering fluxes of AVFs. However, the exact surface age of
63 volcanic areas is rarely mapped in detail, but Holocene areas are often reported in geological maps.
64 Here, basalt alkalinity fluxes are related to the calculated Holocene areal proportion of volcanic
65 fields at the catchment scale. For this, the concept of weathering reactivity is introduced, which is
66 the relative alkalinity flux of AVFs to the alkalinity flux estimated for IVFs. This reactivity R is
67 compared with the relative age distribution of surface areas, using the proportion of total area
68 occupied by Holocene lavas. From this comparison a function for the decay of alkalinity fluxes
69 with increasing proportion of older land surface area is derived and discussed.

70

2. Methods

The volcanic fields used to establish the relationship between weathering reactivity and Holocene coverage are predominantly described as basalt areas (Li et al., 2016). Based on the availability of detailed geological maps, 33 volcanic provinces were selected, with 19 IVFs and 14 AVFs. A detailed description is given in the supplementary information. The 14 AVFs are geographically widespread and diverse (Fig.1a). If the absolute age distribution of the volcanic rocks is available, the Holocene areas were mapped using the age range from 11.7 ka to present, according to the International Commission on Stratigraphy version 2017/02 (Cohen et al., 2013). If possible, coordinates of water sample locations were used to constrain catchment boundary to calculate the Holocene fraction for monitored areas. In all cases already existing alkalinity flux calculations were taken from Li et al. (2016). Detailed information on additional mapping and calculations for each system can be found in the supplementary information (SI).

The weathering reactivity (R) of each volcanic field is calculated by normalizing the observed alkalinity flux of the AVF ($F_{calculated}$, in 10^6 mol km^{-2} a^{-1}) to that of the expected flux if the AVF would be an IVF ($F_{expected}$):

$$R = \frac{F_{calculated}}{F_{expected}} \tag{eq.1}$$

where the expected alkalinity flux $F_{expected}$ for IVFs is given by the function (Fig. 1b):

$$F_{expected}\ (10^6\ mol\ km^{-2}a^{-1}) =\ 0.23 * e^{(0.06*T\ (°C))}, \text{ standard deviation} = 0.3 \tag{eq.2}$$

The parameters of the equation were derived by using a Monte Carlo method, simulating 10,000 runs (for more information see Supplementary Information).
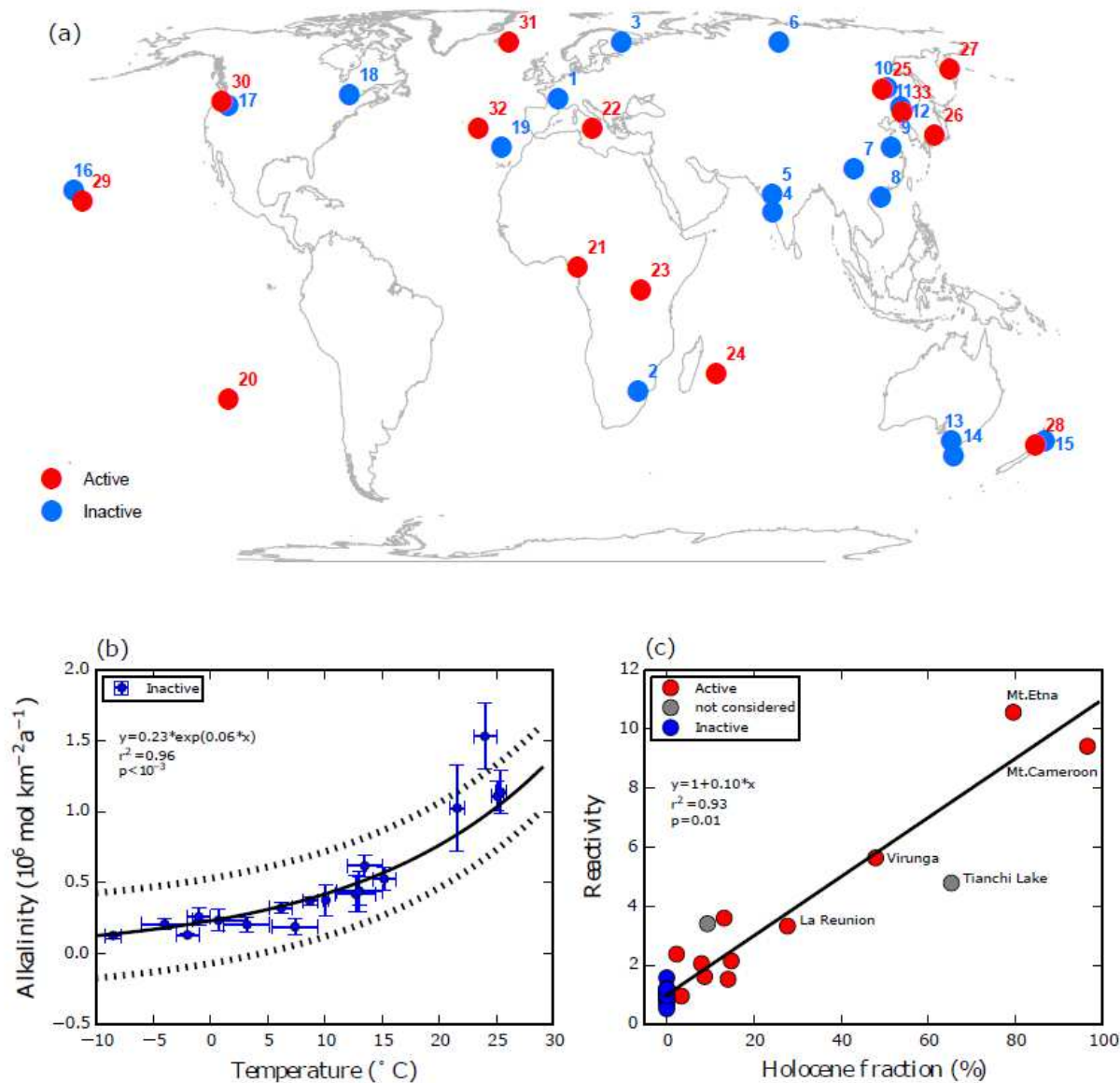
Figure 1(a) The global map shows the locations of the Active Volcanic Fields (in red) and the Inactive Volcanic Fields (in blue) used in this study (1.Massif Central, 2.South Africa, 3.Karelia, 4.Coastal Deccan, 5.Interior Deccan, 6.Siberia Traps, 7.E'Mei, 8.Lei-Qiong, 9.Nanjing, 10.Xiaoxinganling, 11.Tumen River, 12.Mudan River, 13.SE Australia, 14.Tasmania, 15.North Island, NZ, 16.Kauai, Hawaii, 17.Columbia Plateau, 18.NE America, 19.Madeira Island, 20.Easter Island, 21.Mt.Cameroon, 22.Mt.Etna, 23.Virunga, 24.La Réunion, 25.Wudalianchi Lake, 26.Japan, 27.Kamchatka, 28.Taranaki, 29.Big Island, Hawaii, 30.High Cascades, 31.Iceland, 32.Sao Miguel, 33.Tianchi Lake). (b) The exponential relationship between area specific alkalinity flux rates and the land surface temperature for IVFs. The dashed lines represent the range of the mean residual standard deviation of the function (see Supplementary Information). Note that r² and the p-value were derived by a linear regression of calculated alkalinity flux rates

4

vs. estimated alkalinity flux rates using the new scaling law. (c) The relationship between the Holocene area fraction of the used watersheds from the volcanic fields and the weathering reactivity R. Note that "Tianchi Lake" and "Sao Miguel" are excluded from the calculation of the regression line because the applied catchments where not dominated by basalt but by trachytic volcanic rock types. Both data points still seem to follow the identified regression trend line for AVFs. R² and p-value were calculated by a linear regression of the Holocene fraction vs. reactivity for all AVFs.

93   IVFs group around a reactivity R=1 in Fig. 1c, while having a Holocene fraction of zero. The
94   reactivity R (eq. 1) of an AVF can be estimated by the Holocene area fraction as implied by the
95   significant linear correlation identified in Fig. 1c. The theoretical reactivity of a 100% Holocene
96   area H might be estimated by the equation given by Fig. 1c substituting y and x and setting H to
97   100:

98
99    $R_{100\% \ Holocene} = 1 + 0.10 * H = 11$ (eq.3)
100

101   And with this the flux from a young system of only Holocene age:

102
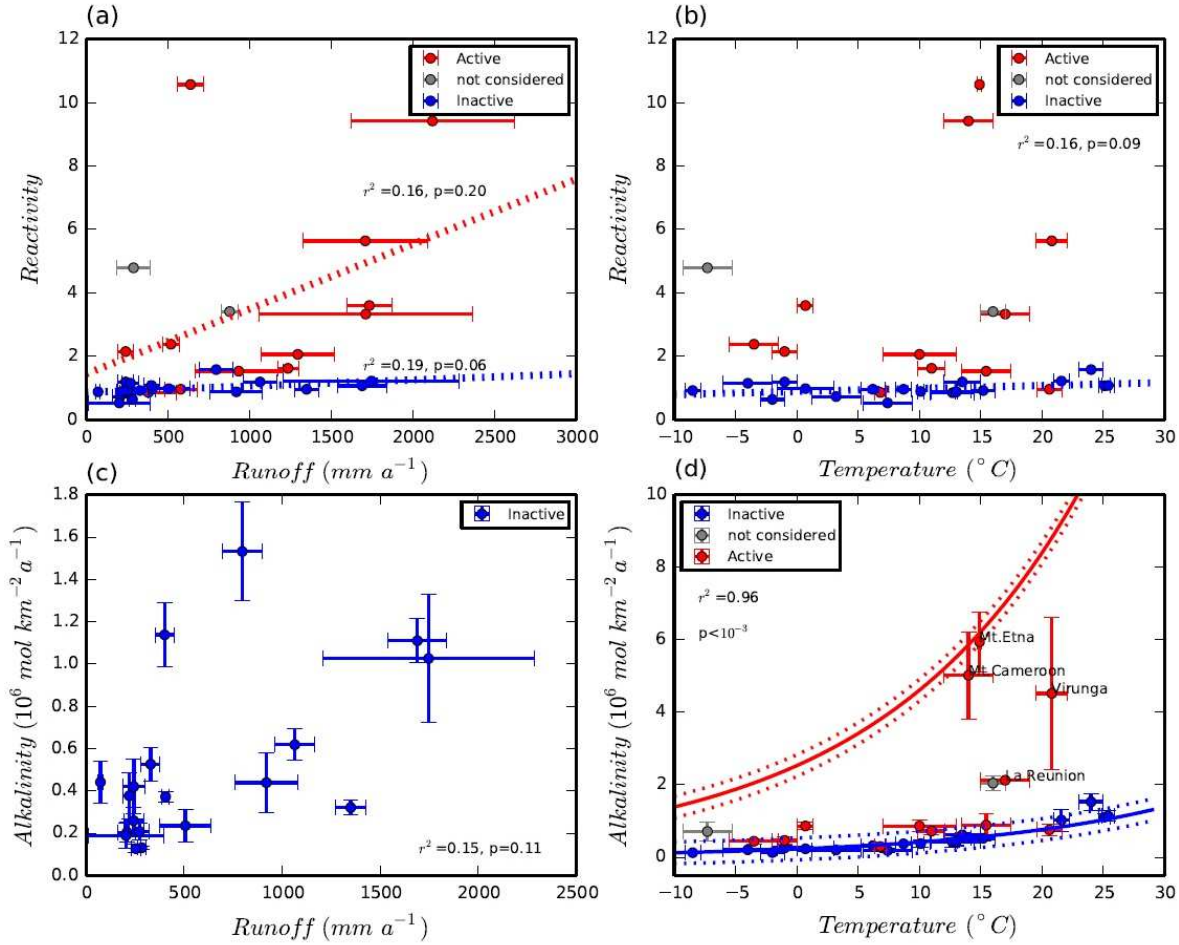103 $F_{Holocene} = R_{100\% \ Holocene} * F_{expected}$ (eq.4)
104

105

Figure 2(a) shows the runoff-reactivity relationship of all studied volcanic fields. The blue regression line (IVFs) suggests almost no correlation of reactivity with runoff, also for the AFVs no significant correlation is identified (coefficient of determination r²=0.16 (p=0.20)) (b) Reactivity versus temperature suggests no bias of reactivity due to a temperature effect for AVFs, as reactivity is based on a temperature normalized parameterization. For the IVFs (r²=0.16, p=0.09) no bias with temperature can be identified due to the good correlation of alkalinity fluxes with land surface temperature (blue line) (c) Runoff versus alkalinity flux rates for inactive volcanic fields shows no significant correlation (r²=0.15, p=0.11) (d) Temperature versus alkalinity flux rates for all volcanic fields of the study. The blue line represents the new scaling law for IVFs and the red line the new scaling law for AVFs with 100% Holocene area coverage (calculated deviation is represented by dashed lines). R² and p-value are derived by a linear regression of calculated alkalinity flux rates vs. observed alkalinity flux rates for all volcanic fields.

Global alkalinity fluxes from basalt areas were calculated by using equation 2 for older areas than of Holocene age and equation 4 for mapped Holocene areas. These equations (eq.2 and following,

110 using information based on eq.2) were calibrated for areas with a runoff > 74 mm a^{-1} (lowest runoff
111 value in data compilation of Li et al. (2016) and therefore limit of the model setup) to avoid too
112 high alkalinity fluxes from drier areas with high temperature (*e.g.*, the Sahara Desert), assuming
113 that neglecting fluxes from areas with lower runoff are not biasing the comparison (Tab. S1,
114 supplementary information). In this case an overestimation is avoided. For the global calculation
115 of CO_2 consumption by the new scaling law, a Monte Carlo method simulating 10,000 runs was
116 applied (see supplement information).

117 Results are compared with four previous global empirical alkalinity flux models (Bluth and Kump,
118 1994; Amiotte-Suchet and Probst, 1995; Dessert et al., 2003; Goll et al., 2014). Alkalinity fluxes
119 were translated into CO_2 consumption to allow for comparison with previous literature. For all
120 models the same data input was used: a newly compiled global basalt map (mostly derived by the
121 basalt lithological layer from the GLiM, but enhanced by mapped Holocene areas (SI; Hartmann
122 and Moosdorf, 2012), additional regional geological maps describing basalt areas and the maps of
123 the volcanic fields used in this study, for detailed information see supplementary information),
124 temperature (Hijmans et al., 2005) and runoff (Fekete et al., 2002).

125

3. Results and Discussion

127 Studied IVFs are characterized by a Holocene volcanic surface area of 0% with weathering
128 reactivity R ranging between 0.5 and 1.6 (Fig. 1c). In contrast, AVFs show a large range of
129 Holocene coverage, from 0.2% (High Cascades) to 96.6% (Mount Cameroon), and weathering
130 reactivity between 0.9 (High Cascades) and 10.6 (Mount Etna). The weathering reactivity
131 correlates strongly with the percentage of Holocene area ($r^2 = 0.93$; Fig. 1c), suggesting Holocene
132 surface area distribution to be a good predictor for the enhanced alkalinity fluxes from a volcanic
133 system:

134 $F_{alkalinity} = (1 + 0.10 * H) * 0.23 * e^{(0.06*T)}$ [$10^6 \ mol \ km^{-2}a^{-1}$], standard deviation = 0.3   (eq.5)

135 where H is the Holocene fraction of a volcanic system in % and T is land surface temperature in
136 °C.

137 The Holocene fraction is not interpreted as the physical cause for elevated alkalinity fluxes.
138 Instead, magmatic CO_2 contribution, geothermal-hydrothermal activity and the input of new
139 volcanic material on top of the surface (properties and "freshness" of the surface area for reaction)
140 are contributing to enhanced alkalinity fluxes. Volcanic ashes and ejecta might contribute to
141 elevated weathering fluxes because of a relatively high content of glass. Glass dissolution rates are
142 relatively high compared to mineral dissolution rates in general, but base cation content release
143 varies dependent on the Si:O ratio (Wolff-Boenisch et al., 2006).

The magmatic CO_2 contributions to alkalinity fluxes in young volcanic systems may be large in general, but data are scarce to evaluate the global relevance for AVFs. For the Lesser Antilles a magmatic contribution of 23 to 40% to the CO_2 consumed by weathering was identified (Rivé et al., 2013). High ^{13}C-DIC values suggest that magmatic CO_2 contributes significantly to the alkalinity fluxes from the Virunga system (Balagizi et al., 2015). The magmatic CO_2 contribution derived from volcanic calcite dissolution on Iceland was estimated to be about 10% of the alkalinity fluxes for the studied area (Jacobson et al., 2015). In case of the Etna 7% of the CO_2 emitted due to volcanic activity may be captured by weathering (Aiuppa et al., 2000). These examples suggest that significant amounts of magmatic carbon may be transferred to the ocean directly via intra-volcanic weathering from AVFs.

These examples show that in case of active volcanic fields the traditional view on kinetic versus supply limitation in the "shallow" critical zone in context of tectonic settings does not hold (e.g., Ferrier et al., 2016). In contrary the supply of fresh material on top of the classical critical zone and the weathering from below the classical critical zone, suggests that these hot spots of silicate weathering in active volcanic areas, which contribute over proportionally to the global CO_2 consumption by silicate weathering, demand likely a different way of looking at it. The blue data points (IVF) in Figure 2d suggest a kinetic limited regime and follow a temperature dependency. The red points (AVF) however are located above the data points of IVF in general. Taking into account that the four AVFs Mt. Etna, Mt. Cameroon, Virunga and La Reunion have the highest Holocene fractions (96.6%-27.7%) and that the further AVFs, which have less than 15% Holocene coverage are located in general above the regression line for IVFs, supports the argument that a combination of elevated geothermal fluxes, magmatic CO_2 and fresh material supplied on top of the classical critical zone contribute to the observed elevated alkalinity fluxes for AVFs in general.

The calculated global basalt weathering alkalinity fluxes based on previous global models (Bluth and Kump, 1994; Amiotte-Suchet and Probst, 1995; Dessert et al., 2003; Goll et al., 2014) give alkalinity fluxes ranging between 0.8 to 1.7×10^{12} mol a^{-1}. These values are different to previously published results based on the same models because a different geological map and climate data are used in this study. The new scaling law calculation based on the temperature dependence of weathering rate and the age dependence of weathering reactivity (eq. 4) results in higher global alkalinity fluxes of 1.9×10^{12} mol a^{-1} and 3.3×10^{12} mol a^{-1} for regions with > 74mm a^{-1} runoff, and for all areas, respectively. The latter higher estimate is mainly due to the modeled contribution from dry and hot regions and shows that it is relevant to apply the runoff cut off.

Using the introduced new approach, considering the aging of a volcanic system, reveals that alkalinity fluxes from Holocene areas contribute today only 5% to the global basalt weathering alkalinity flux. This is because so far identified mapped Holocene volcanic areas cover only ~1% of all basalt areas. This study did not include areas of less mafic volcanic areas, like andesites, or middle American volcanics.

The Holocene area is probably underestimated due to information gaps in the reported age information of the global map. The strong dependence of weathering reactivity on relative age of the surface of a considered volcanic system suggests that it is relevant to know the global spatial age distribution of volcanic areas in more detail. Therefore, a new global review of the age distribution of basalt areas would be needed, which is beyond the scope of this study. The lithologies, predominantly described as basaltic in the global map, might introduce an additional bias to the global calculations because heterogeneities in the lithology cannot be excluded. Two active volcanic fields (Sao Miguel and Tianchi Lake) were excluded from the calculation of the scaling law function because available catchments with alkalinity data hold largely lithologies of trachytic composition. Nevertheless, their data points (Fig. 1c) seem to show the same weathering behavior.

Table 1: Summary of CO_2 consumption rates for global basaltic areas applying different models and the new parameterization. For simplicity it was assumed that alkalinity fluxes equal CO_2 consumption. The percentiles of the values of the global calculation by the new scaling law (Monte Carlo method) can be found in the supplement information. The standard deviation is represented by "New scaling law – std" as described in the SI.

Models for comparison	parameters	Global CO_2 consumption rate (10^9 mol/a) for limited area in comparison (only areas with > 74mm/a runoff)	Global CO_2 consumption rate (10^9 mol/a)
Dessert et al. 2003	runoff, temperature	1669	1684
Amiotte-Suchet & Probst, 1995	runoff	863	870
Bluth & Kump, 1994	runoff	746	761
Goll et al., 2014	runoff, temperature	1566	1580
New scaling law	temperature	1930	3300
New scaling law – std (SI)		90	200

The applied time period of the Holocene boundary suggests that the aging of the "weathering motor" of a basaltic volcanic area, including internal weathering, with declining volcanic activity is rather rapid. This implies that peaks in global volcanic activity have probably a short but intensive effect on the CO_2 consumption. A pronounced effect on the global carbon cycle by shifting the global reactivity of volcanic areas may only be relevant for geological periods with significantly elevated production of new volcanic areas, accompanied by geothermal-hydrothermal activity and capture of magmatic CO_2 before its escape to the atmosphere.

Results may have relevance for the carbon cycle and climate studies exploring the emplacement of large igneous provinces like the CAMP (Schaller et al., 2012) or the Deccan traps (Caldeira and

Rampino, 1990) with production of large basaltic areas within a short time. However, the biological contribution to CO_2 drawdown, via elevated fertilization effects, *e.g.* P- or Si-release due to weathering and elevated CO_2 in the atmosphere should be taken into account, too.

Looking deeper into Earth's history: variations in the solid Earth CO_2 degassing rate or changes in environmental conditions affecting the weathering intensity (Teitler et al., 2014; Hartmann et al., 2017) may have caused different reactivity patterns in dependence of surface age as shown here.

In conclusion, a simple approach to detect an aging effect, using surface age as a proxy for several combined processes, was chosen due to availability of data. It can be shown that there exists a linear relationship between temperature normalized alkalinity fluxes and the Holocene area fraction of a volcanic system. Nevertheless, the combined effect on elevated weathering reactivity due to magmatic CO_2 contribution, hydrothermal activity, production of fresh surface area for reaction, and hydrological factors of young volcanic systems remains to be disentangled, for single volcanic systems, as well as for the emplacement of larger, trap-style basalt areas.

6. References

Aiuppa, A., Allard, P., D'Alessandro, W., Michel, A., Parello, F., Treuil, M., and Valenza, M.: Mobility and fluxes of major, minor and trace metals during basalt weathering and groundwater transport at Mt. Etna volcano (Sicily), Geochimica et Cosmochimica Acta, 64, 1827-1841, 2000.

Amiotte-Suchet, P., and Probst, J. L.: A global model for present-day atmospheric/soil CO2 consumption by chemical erosion of continental rocks (GEM-CO2), Tellus B, 47, 273-280, 10.1034/j.1600-0889.47.issue1.23.x, 1995.

Balagizi, C. M., Darchambeau, F., Bouillon, S., Yalire, M. M., Lambert, T., and Borges, A. V.: River geochemistry, chemical weathering, and atmospheric CO2 consumption rates in the Virunga Volcanic Province (East Africa), Geochemistry, Geophysics, Geosystems, 16, 2637-2660, 10.1002/2015GC005999, 2015.

Berner, R. A., Lasaga, A. C., and Garrels, R. M.: The carbonate-silicate geochemical cycle and its effect on atmospheric carbon dioxide over the past 100 million years, Am J Sci, 283, 641-683, 1983.

Bluth, G. J., and Kump, L. R.: Lithologic and climatologic controls of river chemistry, Geochimica et Cosmochimica Acta, 58, 2341-2359, 1994.

Caldeira, K., and Rampino, M. R.: Carbon dioxide emissions from Deccan volcanism and a K/T boundary greenhouse effect, Geophysical Research Letters, 17, 1299-1302, 1990.

241 Cohen, K., Finney, S., Gibbard, P., and Fan, J.-X.: The ICS international chronostratigraphic chart,
242   Episodes, 36, 199-204, 2013.
243 Coogan, L. A., and Dosso, S. E.: Alteration of ocean crust provides a strong temperature dependent
244   feedback on the geological carbon cycle and is a primary driver of the Sr-isotopic composition of
245   seawater, Earth and Planetary Science Letters, 415, 38-46,
246   http://dx.doi.org/10.1016/j.epsl.2015.01.027, 2015.
247 Dessert, C., Dupré, B., François, L. M., Schott, J., Gaillardet, J., Chakrapani, G., and Bajpai, S.: Erosion of
248   Deccan Traps determined by river geochemistry: impact on the global climate and the 87Sr/86Sr
249   ratio of seawater, Earth and Planetary Science Letters, 188, 459-474,
250   http://dx.doi.org/10.1016/S0012-821X(01)00317-X, 2001.
251 Dessert, C., Dupré, B., Gaillardet, J., François, L. M., and Allègre, C. J.: Basalt weathering laws and the
252   impact of basalt weathering on the global carbon cycle, Chemical Geology, 202, 257-273,
253   http://dx.doi.org/10.1016/j.chemgeo.2002.10.001, 2003.
254 Fekete, B. M., Vörösmarty, C. J., and Grabs, W.: High‐resolution fields of global runoff combining
255   observed river discharge and simulated water balances, Global Biogeochemical Cycles, 16, 2002.
256 Ferrier, K. L., Riebe, C. S., and Jesse Hahm, W.: Testing for supply‐limited and kinetic‐limited chemical
257   erosion in field measurements of regolith production and chemical depletion, Geochemistry,
258   Geophysics, Geosystems, 17, 2270-2285, 2016.
259 Gaillardet, J., Dupré, B., Louvat, P., and Allègre, C. J.: Global silicate weathering and CO2 consumption
260   rates deduced from the chemistry of large rivers, Chemical Geology, 159, 3-30,
261   http://dx.doi.org/10.1016/S0009-2541(99)00031-5, 1999.
262 Gaillardet, J., Rad, S., Rivé, K., Louvat, P., Gorge, C., Allègre, C. J., and Lajeunesse, E.: Orography-driven
263   chemical denudation in the Lesser Antilles: Evidence for a new feed-back mechanism stabilizing
264   atmospheric CO2, American journal of science, 311, 851-894, 2011.
265 Goddéris, Y., Donnadieu, Y., Nédélec, A., Dupré, B., Dessert, C., Grard, A., Ramstein, G., and François, L.
266   M.: The Sturtian 'snowball' glaciation: fire and ice, Earth and Planetary Science Letters, 211, 1-12,
267   http://dx.doi.org/10.1016/S0012-821X(03)00197-3, 2003.
268 Goll, D. S., Moosdorf, N., Hartmann, J., and Brovkin, V.: Climate-driven changes in chemical weathering
269   and associated phosphorus release since 1850: Implications for the land carbon balance,
270   Geophysical Research Letters, 41, 3553-3558, 10.1002/2014GL059471, 2014.
271 Hartmann, J., Jansen, N., Dürr, H. H., Kempe, S., and Köhler, P.: Global CO2-consumption by chemical
272   weathering: What is the contribution of highly active weathering regions?, Global and Planetary
273   Change, 69, 185-194, 2009.
274 Hartmann, J., and Moosdorf, N.: The new global lithological map database GLiM: A representation of
275   rock properties at the Earth surface, Geochemistry, Geophysics, Geosystems, 13, n/a-n/a,
276   10.1029/2012gc004370, 2012.
277 Hartmann, J., Li, G., and West, A. J.: Running out of gas: Zircon 18O-Hf-U/Pb evidence for Snowball Earth
278   preconditioned by low degassing, Geochemical Perspectives Letters, 4, 41-46,
279   http://dx.doi.org/10.7185/geochemlet.1734, 2017.
280 Hijmans, R. J., Cameron, S. E., Parra, J. L., Jones, P. G., and Jarvis, A.: Very high resolution interpolated
281   climate surfaces for global land areas, International journal of climatology, 25, 1965-1978, 2005.
282 Jacobson, A. D., Grace Andrews, M., Lehn, G. O., and Holmden, C.: Silicate versus carbonate weathering
283   in Iceland: New insights from Ca isotopes, Earth and Planetary Science Letters, 416, 132-142,
284   http://dx.doi.org/10.1016/j.epsl.2015.01.030, 2015.
285 Kent, D. V., and Muttoni, G.: Modulation of Late Cretaceous and Cenozoic climate by variable drawdown
286   of atmospheric pCO2 from weathering of basaltic provinces on continents drifting through the
287   equatorial humid belt, Clim. Past, 9, 525-546, 10.5194/cp-9-525-2013, 2013.

288 Li, G., and Elderfield, H.: Evolution of carbon cycle over the past 100 million years, Geochimica et
289   Cosmochimica Acta, 103, 11-25, http://dx.doi.org/10.1016/j.gca.2012.10.014, 2013.
290 Li, G., Hartmann, J., Derry, L. A., West, A. J., You, C.-F., Long, X., Zhan, T., Li, L., Li, G., Qiu, W., Li, T., Liu,
291   L., Chen, Y., Ji, J., Zhao, L., and Chen, J.: Temperature dependence of basalt weathering, Earth and
292   Planetary Science Letters, 443, 59-69, http://dx.doi.org/10.1016/j.epsl.2016.03.015, 2016.
293 Rad, S., Rivé, K., Vittecoq, B., Cerdan, O., and Allègre, C. J.: Chemical weathering and erosion rates in the
294   Lesser Antilles: An overview in Guadeloupe, Martinique and Dominica, Journal of South American
295   Earth Sciences, 45, 331-344, http://dx.doi.org/10.1016/j.jsames.2013.03.004, 2013.
296 Rivé, K., Gaillardet, J., Agrinier, P., and Rad, S.: Carbon isotopes in the rivers from the Lesser Antilles:
297   origin of the carbonic acid consumed by weathering reactions in the Lesser Antilles, Earth Surface
298   Processes and Landforms, 38, 1020-1035, 10.1002/esp.3385, 2013.
299 Schaller, M. F., Wright, J. D., Kent, D. V., and Olsen, P. E.: Rapid emplacement of the Central Atlantic
300   Magmatic Province as a net sink for CO2, Earth and Planetary Science Letters, 323–324, 27-39,
301   http://dx.doi.org/10.1016/j.epsl.2011.12.028, 2012.
302 Taylor, A., and Blum, J. D.: Relation between soil age and silicate weathering rates determined from the
303   chemical evolution of a glacial chronosequence, Geology, 23, 979-982, 1995.
304 Teitler, Y., Le Hir, G., Fluteau, F., Philippot, P., and Donnadieu, Y.: Investigating the Paleoproterozoic
305   glaciations with 3-D climate modeling, Earth and Planetary Science Letters, 395, 71-80,
306   http://dx.doi.org/10.1016/j.epsl.2014.03.044, 2014.
307 Walker, J. C. G., Hays, P. B., and Kasting, J. F.: A negative feedback mechanism for the long-term
308   stabilization of Earth's surface temperature, Journal of Geophysical Research: Oceans, 86, 9776-
309   9782, 10.1029/JC086iC10p09776, 1981.
310 Wolff-Boenisch, D., Gislason, S. R., and Oelkers, E. H.: The effect of crystallinity on dissolution rates and
311   CO2 consumption capacity of silicates, Geochimica et Cosmochimica Acta, 70, 858-870, 2006.

312